Prethermal quasiconserved observables in Floquet quantum systems

Chao Yin,[1,*,†] Pai Peng (彭湃),[2,†] Xiaoyang Huang,[1] Chandrasekhar Ramanathan,[3] and Paola Cappellaro[4,1,‡]

[1]*Research Laboratory of Electronics, Massachusetts Institute of Technology, Cambridge, Massachusetts 02139, USA*

[2]*Department of Electrical Engineering and Computer Science, Massachusetts Institute of Technology, Cambridge, Massachusetts 02139, USA*

[3]*Department of Physics and Astronomy, Dartmouth College, Hanover, New Hampshire 03755, USA*

[4]*Department of Nuclear Science and Engineering, Massachusetts Institute of Technology, Cambridge, Massachusetts 02139, USA*

(Received 21 May 2020; revised 27 January 2021; accepted 28 January 2021; published 15 February 2021)

Prethermalization, by introducing emergent quasiconserved observables, plays a crucial role in protecting periodically driven (Floquet) many-body phases over an exponentially long time, while the ultimate fate of such quasiconserved operators can signal thermalization to infinite temperature. To elucidate the properties of prethermal quasiconservation in many-body Floquet systems, here we systematically analyze infinite-temperature correlations between observables. We numerically show that the late-time behavior of the autocorrelations unambiguously distinguishes quasiconserved observables from nonconserved ones, allowing one to single out a set of linearly independent quasiconserved observables. By investigating two Floquet spin models, we identify two different mechanisms underlying the quasiconservation law. First, we numerically verify energy quasiconservation when the driving frequency is large, so that the system dynamics is approximately described by a static prethermal Hamiltonian. More interestingly, under moderate driving frequency, another quasiconserved observable can still persist if the Floquet driving contains a large global rotation. We show theoretically how to calculate this conserved observable and provide numerical verification. Having systematically identified all quasiconserved observables, we can finally investigate their behavior in the infinite-time limit and thermodynamic limit, using autocorrelations obtained from both numerical simulation and experiments in solid-state nuclear magnetic resonance systems.

DOI: 10.1103/PhysRevB.103.054305

I. INTRODUCTION

Controlling quantum systems using a periodic (Floquet) drive has emerged as a powerful tool in the field of condensed-matter physics and quantum information science. It has been used to realize Hamiltonians that are not accessible in a static system, such as modifying the tunneling and coupling rates [1–6], inducing nontrivial topological structures [7–17], creating synthetic gauge fields [18–22], and spin-orbit couplings [23]. On a quantum computer, Floquet engineering also enables universal quantum simulation via the Trotter-Suzuki scheme [24–30]. Floquet systems also possess interesting dynamical phenomena, ranging from the discrete-time crystalline phase [31–35] to dynamical localization [36,37], dynamical phase transitions [38,39], and coherent destruction of tunneling [40–42].

While the connection to an effective time-independent Hamiltonian is appealing, the active drive leads to energy absorption by the Floquet many-body system, which is then expected to heat up to infinite temperature. The heating is detrimental to any quantum application, as no local quantum information is retained and all interesting phenomena mentioned above disappear [43–45]. It has been shown theoretically [46–50] and experimentally [51,52] that even when the system heats up, the thermalization time can be exponentially long in the drive parameters (typically the frequency of a rapid drive). Then, a long-lived *prethermal* quasiequilibrium is established, which allows exploitation of the engineered Floquet Hamiltonian for quantum simulation [53–55]. The emergent symmetries and conserved observables in the prethermal state distinguish it from the fully thermalized state and underpin the existence of novel Floquet phases [34,35,50]. Even more surprisingly, some numerical studies have shown that the emergent conserved observables might not display thermalizing behavior even in the infinite-time limit [53–56]. Many-body localization [32,57–63], dynamic localization [53,55,64], and some fine-tuned driving protocols [54,56,65] provide a way to escape the thermalization fate, which could also be absent in finite-size systems. Indeed, distinguishing the long-lived prethermal state from an eventual thermal state is challenging. Numerical studies are bound to finite-size (and often small) systems, while experiments can only probe finite times, before the external environment induces thermal relaxation.

Here we tackle this problem by a numerical and experimental study of two Floquet models in spin chains, namely, the kicked dipolar model (KDM) and the alternating dipolar model (ADM). While most studies on spin chain dynamics have focused on the evolution of pure states, here we propose to study Floquet prethermalization using infinite-temperature correlations. This metric provides information about quasi-

*yinchao1998@pku.edu.cn

†These authors contributed equally to this work.

‡pcappell@mit.edu

conserved observables across the whole spectrum and serves as a direct measurable quantity in nuclear magnetic resonance (NMR) experiments. In Sec. II, we show that the existence of long-lived quasiconserved observables can be unambiguously identified using late-time behavior of the correlations, based on which we provide a method to systematically search for all linearly independent local quasiconserved quantities. Then we provide both numerical and analytical tools to investigate such prethermal conserved observables and their origins. We first show that the prethermal Hamiltonian $H_{\rm pre}$ obtained from the Magnus expansion under rapid drive yields a quasiconserved observable in each model, in Sec. III A. We further show, in Sec. III B, that when the driving Hamiltonian contains a large global rotation, the Floquet propagator can induce an additional conserved observable, as shown by going beyond the usual Magnus expansion. With all the quasiconserved observables at hand, we investigate, in Sec. IV, whether they exist in the thermodynamic limit and infinite-time limit by looking at the dependence of autocorrelations on system size (numerically) and on time (experimentally). Both methods indicate that quasiconserved observables vanish and the system thermalizes to infinite temperature.

II. QUASICONSERVED OBSERVABLES

A. Hamiltonians and correlations

In this paper, we use the Trotter-Suzuki scheme for the driving protocol, where the time-dependent Hamiltonian is piecewise constant in one driving period. However, our results are general for any form of periodic driving. The evolution of the system that we study is given by the unitary propagator in one period, $U_F = e^{-iH_2\tau}e^{-iH_1\tau}$, where in each period we consider the system to be under the Hamiltonian H_1 for a time τ, and then under H_2 for another duration τ. Motivated by NMR experiments, we consider two models of an L-site spin-1/2 chain: the kicked dipolar model (KDM), where $H_1^{(K)} = JD_y$ and $H_2^{(K)} = hZ$, and the alternating dipolar model (ADM), where $H_1^{(A)} = JD_y$ and $H_2^{(A)} = JD_x$. Here, $D_\alpha = \sum_{j<k} \frac{1}{2}(3S_\alpha^j S_\alpha^k - \vec{S}_j \cdot \vec{S}_k)/|j-k|^3$ is the dipolar interaction operator in an arbitrary direction set by α ($\alpha = x, y, z$), where S_α^j are spin-1/2 operators of the jth spin ($j = 1, \ldots, L$) and $\vec{S}_j = (S_x^j, S_y^j, S_z^j)^T$. As shown in Ref. [35], the $1/r^3$ interaction is sufficiently short range in one dimension (1D) to yield no qualitative difference with respect to the nearest-neighbor interaction, and thus for simplicity in numerical and analytical studies we only keep the nearest-neighbor interaction unless explicitly mentioned. $Z = \sum_j S_z^j$ is the collective magnetization operator along the z axis, and below we will also use $X = \sum_j S_x^j$, $Y = \sum_j S_y^j$. J and h are the strength of the dipolar interaction and the collective z field, respectively, and we fix $h = J$ throughout the paper. In numerics, we assume periodic boundary conditions.

To investigate the quasiconservation properties, we use infinite-temperature correlations as our metric, $\langle \mathcal{O}(t)\mathcal{O}'\rangle_{\beta=0} \equiv \mathrm{Tr}[U_t \mathcal{O} U_t^\dagger \mathcal{O}']/(\|\mathcal{O}\|\|\mathcal{O}'\|)$, where U_t is the unitary evolution during time t, $\mathcal{O}$ and $\mathcal{O}'$ are observables, and the norm is defined as $\|\mathcal{O}\| \equiv \sqrt{\mathrm{Tr}\mathcal{O}^2}$ [66]. Note that early works [67] used this metric to determine whether a system is ergodic or integrable. Here we show that we can also use these correlations to identify quasiconservation in prethermal systems, even if they are expected to be ergodic.

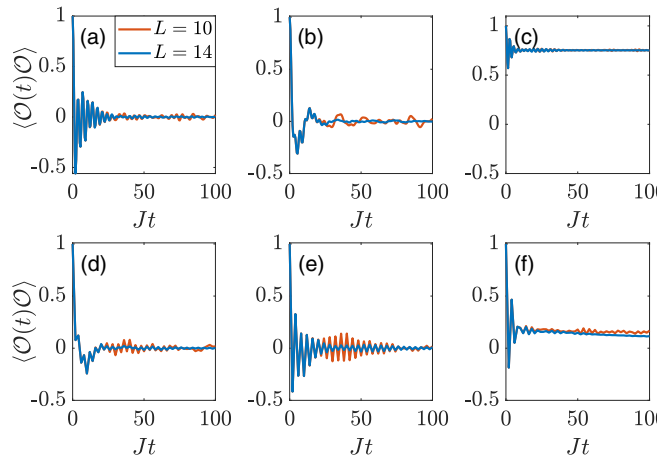

FIG. 1. Typical dynamics of $\langle \mathcal{O}(t)\mathcal{O}'\rangle$ in a Floquet spin chain. Here we choose KDM and $\mathcal{O} = \mathcal{O}'$. (a)–(c) $J\tau = 0.5$; (d)–(f) $J\tau = 2$. (a),(d) $\mathcal{O} = X$; (b),(e) $\mathcal{O} = Y$; (c),(f) $\mathcal{O} = Z$. Different colors correspond to different system size L, as shown in the legend.

Figure 1 shows numerical simulations of some exemplary correlations, i.e., the magnetization along three axes $\mathcal{O} = \mathcal{O}' = Z, X, Y$ in KDM (the qualitative behavior is general for other observables and models.) The autocorrelations of X and Y display oscillations around 0 and damping, which originate from the z field and the dipolar interaction, respectively. Instead, $\langle Z(t)Z\rangle$ exhibits a more interesting behavior. For small $J\tau$, it quickly equilibrates at a nonzero value independent of L, and it remains constant afterwards. For relatively large $J\tau$, there is a slow decay of $\langle Z(t)Z\rangle$ toward a final value that decreases with increasing L. We thus expect the final value to be zero in the thermodynamic limit, corresponding to an infinite-temperature final state. Indeed, the observable Z displays the defining characteristics of what we deem a quasiconserved observable in the prethermal regime: the autocorrelation of a quasiconserved observable is nonzero in the prethermal regime, but goes to zero in the fully thermalized state. In simulations, autocorrelations of quasiconserved observables still have nonzero value at infinite time due to the small system size [e.g., $\langle Z(t)Z\rangle$ in Fig. 1], while for nonconserved observables, autocorrelations are zero [e.g., $\langle X(t)X\rangle$ in Fig. 1]. These distinct behaviors serve as a direct metric to identify quasiconserved observables. As any observable that overlaps with a quasiconserved observable would have nonzero infinite-time autocorrelation, we want to find a linearly independent, orthogonal set of *eigen*quasiconserved observables.

B. Eigenquasiconserved observables

We design a systematic procedure to search for the set of eigenquasiconserved observables, $\{\mathcal{E}_\mu\}$, starting from the infinite-time correlations $\langle \mathcal{O}(\infty)\mathcal{O}'\rangle \equiv \lim_{T\to\infty}(1/T)\int_0^T \langle \mathcal{O}(t)\mathcal{O}'\rangle dt$. We note that eigenvectors $\{E_\mu\}$ of the Floquet (super)propagator $\hat{U}_F$ form an orthogonal vector basis for the space of operators (here, $\hat{U}[\mathcal{O}] = U\mathcal{O}U^\dagger$) $|\langle E_j(\infty)E_k\rangle| \propto \delta_{jk}$, which we can call "eigenobservables." However, this operator basis is, in general, highly nonlocal

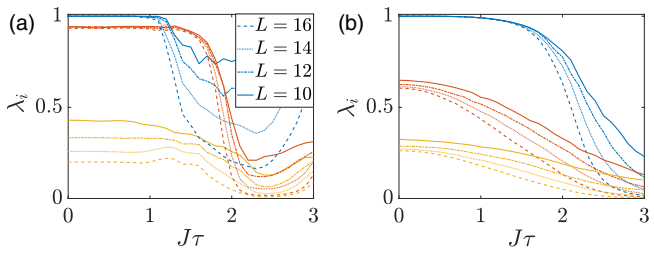

FIG. 2. By considering the matrix Λ obtained for each $J\tau$ Trotter step, we calculate the three largest eigenvalues as a function of $J\tau$ for (a) KDM and (b) ADM. The curve color represents different eigenvalues and the curve style represents different system sizes. From the eigenvalues and their dependence on system size, we see that there are two eigenquasiconserved observables in KDM, while only one in ADM.

and thus not practical. We then want to find a small, local set of observables that approximates the exact eigenobservables and has nonzero eigenvalues, that is, are quasiconserved. We start from a basis set $\{\mathcal{O}_{(\alpha)}\}$ of Hermitian observables that are translationally invariant sums of local operators,

$$\mathcal{O}_{(\alpha)} = \sum_j S^j_{\alpha_1} S^{j+1}_{\alpha_2} \cdots S^{j+r-1}_{\alpha_r}. \tag{1}$$

Here, $(\alpha) \equiv (\alpha_1, \ldots, \alpha_r)$ with $\alpha_k \in \{x, y, z, 0\}$, where S^j_0 denotes the identity matrix operating on the jth spin. By imposing $\alpha_1, \alpha_r \neq 0$, we say $\mathcal{O}_{(\alpha)}$ is of the range of r: each term in $\mathcal{O}_{(\alpha)}$ acts nontrivially on most r neighboring spins. Since the number of operators is exponentially large in system size, we restrict our search to the operator subspace spanned by $\mathcal{O}_{(\alpha)}$ whose range $r \leqslant r_c$, which are local and thus experimentally relevant. Starting from an orthonormal operator basis $\{\mathcal{O}_\mu\}$ of this subspace (with $\langle \mathcal{O}_\mu \mathcal{O}_\nu \rangle = \delta_{\mu\nu}$), we construct a matrix from all pair correlations, $\Lambda_{\mu\nu} = \langle \mathcal{O}_\mu(\infty)\mathcal{O}_\nu \rangle$. The matrix Λ is the projection of the infinite-time propagator $\hat{U}_F(t \to \infty)$ onto the r_c-local subspace. The diagonalization of Λ yields the local eigenobservables $\mathcal{E}_k$, and eigenvalues λ_k, satisfying $\langle \mathcal{E}_k(\infty)\mathcal{E}_l \rangle = \lambda_k \delta_{kl}$. Note that since Λ is not ensured to be unitary, its eigenvalues do not have unit amplitude, $\lambda_k \leqslant 1$. We note that the larger the λ_k, the better $\mathcal{E}_k$ approximates an exactly conserved observable. The correlations $\langle \mathcal{O}(\infty)\mathcal{O}' \rangle$ between any two observables whose locality is bounded by r_c can be directly derived by decomposing the observables onto the $\mathcal{E}_\mu$ basis,

$$\langle \mathcal{O}(\infty)\mathcal{O}' \rangle = \sum_\mu \lambda_\mu \langle \mathcal{O}\mathcal{E}_\mu \rangle \langle \mathcal{E}_\mu \mathcal{O}' \rangle. \tag{2}$$

We apply this systematic procedure to the two models under consideration. The infinite-time limit $\mathcal{O}(\infty)$ is taken by considering the diagonal ensemble of $\mathcal{O}$ (that is, keeping only the diagonal matrix elements of $\mathcal{O}$ in the Floquet energy eigenbasis), which gives the same result as averaging $\mathcal{O}$ over a long time. The results for $r_c = 3$ are shown in Fig. 2. At large Trotter steps τ, most eigenvalues go to zero. The upward trends of the eigenvalues when $J\tau = h\tau \to \pi$ (most pronounced for the largest eigenvalue) are due to the fact that $[e^{-iH_1^{(K)}\tau}, e^{-iH_2^{(K)}\tau}] = 0$ at $J\tau = h\tau \to \pi$, making the system equivalent to a time-independent system. Even for small Trotter steps, most eigenvalues are already small and decrease when increasing system size. However, a few eigenvalues are large and show little dependence on system size. This last group comprises the eigenvalues associated with the eigenquasiconserved observables that govern the nontrivial dynamics at long times.

Based on these results, we find that there are two eigenquasiconserved observables for KDM, $\mathcal{E}_1^{(K)}, \mathcal{E}_2^{(K)}$, and one for ADM, $\mathcal{E}_1^{(A)}$. In both models, $\mathcal{E}_1$ is close to their average Hamiltonian, $\overline{H} = H_1 + H_2$ (blue curves in Fig. 2), while $\mathcal{E}_2^{(K)}$ for KDM is close to D_z [red curves in Fig. 2(a)]. Similar additional conserved quantities were predicted in static models [49]. Here we can more carefully analyze these Floquet quasiconserved observables and describe analytically their origin in the limit of small τ in the next section. Even so, we remark that there is an interesting regime at intermediate τ, where $\mathcal{E}_1^{(K)}, \mathcal{E}_2^{(K)}$ are well conserved, since $\lambda_1^{(K)}, \lambda_2^{(K)}$ are still large, but they deviate from their static ($\tau \to 0$) counterparts. This indicates that the quasiconserved observables truly arise from the Floquet dynamics and are not simply a remnant of the approximated, static Hamiltonian.

III. ANALYTICAL DERIVATION OF CONSERVED OBSERVABLES

A. Prethermal Hamiltonian

It is intuitive to expect that a quasiconserved observable might emerge from energy conservation. Indeed, one can always regard the Floquet evolution as arising from an effective static Hamiltonian by setting $U_F = e^{-i\tau H_F}$ for some Hermitian operator H_F. However, in general, this Hamiltonian is highly nonlocal and thus it is not associated to a local quasiconserved observable. Still, when the driving frequency is large compared to local energy scales (here, J, h), the stroboscopic dynamics is given by a time-independent local prethermal Hamiltonian H_{pre} plus a small correction $\delta H(t)$ [46,48], which may be nonlocal. It is this prethermal Hamiltonian H_{pre} that can be associated with a local quasiconserved observable. H_{pre} can be obtained from the Floquet-Magnus expansion [68,69] truncated at an optimal order m^*,

$$H_{\text{pre}} = \sum_{m=0}^{m^*} \tau^m \Omega_m, \tag{3}$$

where the zeroth-order term is the average Hamiltonian $\Omega_0 = \overline{H} = 1/\tau \int_0^\tau H(t)dt$ and higher-order terms Ω_m involve m nested commutators. Then, for spin chains with nearest-neighbor couplings, the range of Ω_m grows linearly with m.

The truncation m^* is crucial not only to keep the prethermal Hamiltonian local, but also because the series in Eq. (3) diverges for a generic many-body system [48]. The time-dependent correction δH is, however, exponentially small in $1/J\tau$, leading to an exponentially long time t_{pre} for the system to heat up. Thus, for $t < t_{\text{pre}}$, the system effectively prethermalizes to the state $e^{-\beta H_{\text{pre}}}$, where β is determined by the initial state energy, making H_{pre} an eigenquasiconserved observable. Although one should investigate the prethermalization process by studying the dynamics of an infinitely large system at long times approaching infinity, numerically we

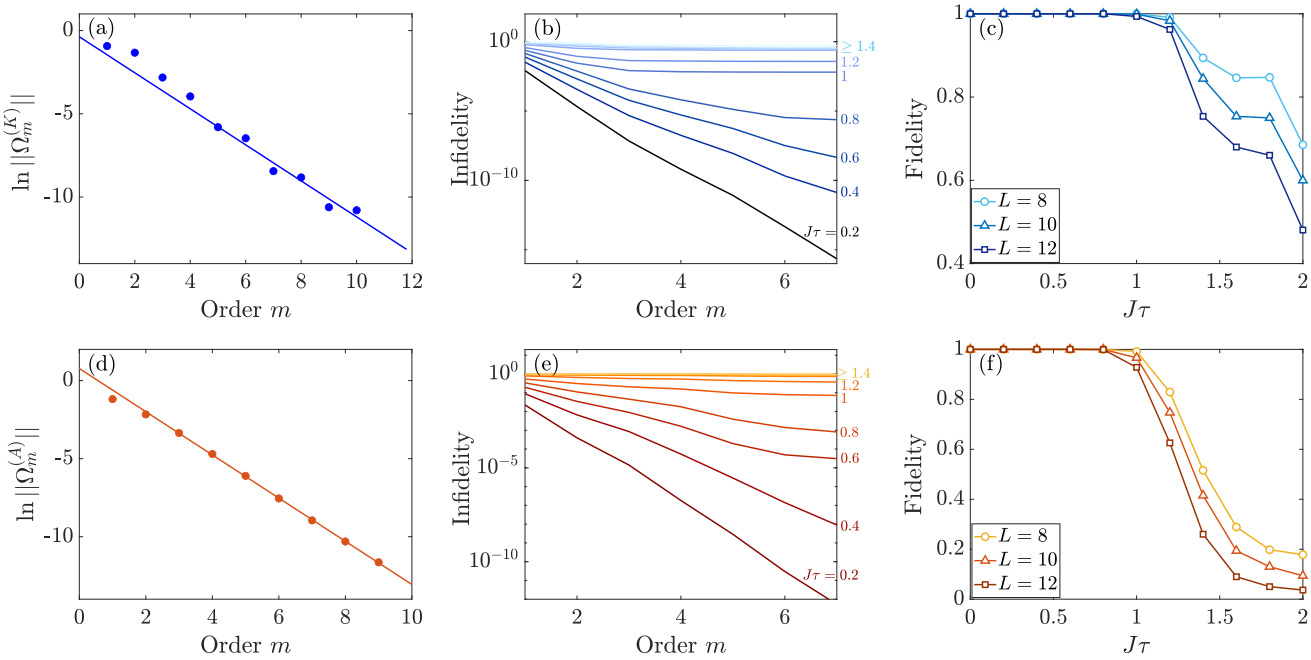

FIG. 3. (a)–(c) The Magnus expansion given by Eq. (3) of KDM; (d)–(f) that of ADM. (a),(d) Circles show the norm of Ω_m (normalized by $L2^L$). The solid line represents the linear fit. (b),(e) Infidelity $1 - \langle H_{\rm pre}(\infty) H_{\rm pre}\rangle$ of infinite-time averaged $H_{\rm pre}$ evaluated up to the mth order. Different curves stand for $J\tau$ from 0.2 to 2, with a step of 0.2. The darker color represents smaller $J\tau$. $L = 12$ is used. (c),(f) Infinite-time autocorrelation of $H_{\rm pre}$ as a function of $J\tau$ for different system sizes. Order $m = 7$.

can only tackle small system sizes, so we take a different approach—we set the time to infinity and study how the observable correlations change when increasing system size. The validity of this approach relies on the fact that for a system size $L < m^*$, the term δH does not appear in the expansion, making $\mathcal{O}_1 = H_{\rm pre}$ exactly conserved even at infinite time for sufficiently small τ. From a physics point of view, this means that the energy $2\pi\hbar/\tau$ is larger than the many-body bandwidth ($\sim JL$), and thus the system cannot absorb energy from the drive if it is faster than $1/JL$. Since the zeroth-order term of $H_{\rm pre}$ is $\overline{H}$, the autocorrelation of $H_{\rm pre}$ provides a bound for that of $\overline{H}$, leading to bounded Trotter error in the Trotter-Suzuki scheme [53].

As further verification, we calculate numerically the Floquet Magnus expansion, given by Eq. (3), up to $m = 10$ and evaluate not only the convergence of the expansion, but also operator conservation. For the first metric, we plot $\|\Omega_m\|$ in Figs. 3(a) and 3(d) for the two models studied. We find that up to the computationally accessible order, the norm of Ω_m decays exponentially, indicating that $H_{\rm pre}$ converges when τ is small. From the slopes in Figs. 3(a) and 3(d), we get radii of convergence $J\tau \approx 3$ for both models. Still, the expansion convergence does not guarantee the resulting $H_{\rm pre}$ is a quasiconserved observable. In Figs. 3(b) and 3(e), we compute the long-time infidelity $(1 - \langle H_{\rm pre}(\infty) H_{\rm pre}\rangle)$ by truncating the expansion in Eq. (3) at increasing orders. When $J\tau$ is small, the autocorrelation exponentially approaches 1 with increasing order, suggesting that the optimal truncation order m^* should be larger than our largest accessible order here, or even absent in the system size we study. Instead, for larger $J\tau$, the correlation stops converging at some order; for even larger $J\tau$ ($J\tau = 1$, for example), the correlation is almost zero for all orders. Therefore, even within the radius of convergence, $J\tau \approx 3$, $H_{\rm pre}$ from Eq. (3) may fail to be quasiconserved. We plot the infinite-time correlation $\langle H_{\rm pre}(\infty) H_{\rm pre}\rangle$ versus $J\tau$ in Figs. 3(c) and 3(f) and show how it changes with system size (here, $H_{\rm pre}$ is evaluated to seventh order). The drop of $\langle H_{\rm pre}(\infty) H_{\rm pre}\rangle$ with increasing system size is evident for $J\tau \gtrsim 1.2$ in both models, suggesting that for the system size we explore, the effective Hamiltonian picture fails in the above parameter space. Note that in the $L \to \infty$ limit, the correlations are expected to be zero for any $\tau > 0$, as will be discussed in Sec. IV.

B. Emergent dipolar order

To search for additional conserved observables in KDM, we develop a method inspired by the existence of discrete time-translation symmetry-protected phases in prethermal Floquet systems [50]. Similar results have been obtained for the static Hamiltonian $\overline{H} = hZ + JD_y$ associated with the (zero-order) KDM. For this model, it has been shown that the polarization Z is quasiconserved and does not reach its thermal equilibrium value until a time that is exponentially long in h/J [49,50,70], even if according to eigenstate thermalization hypothesis (ETH) the system should thermalize.

Since the average Hamiltonian picture breaks down when increasing τ, even though we see from Fig. 2(a) that the second observable is conserved even for larger τ, we must go beyond the static case and work directly on the Floquet system. This kind of system was first studied in [50], where they further focused on the case $h = \pi$ to identify a prethermal Floquet time crystal. Here we generalize their analysis to obtain the novel quasiconserved observable for any h, by

following the intuition in [49]: thanks to the integer spectrum of Z, we expect that there exists a frame where the polarization is conserved up to some small, highly nonlocal corrections in the Hamiltonian. Taking into account the Floquet nature of our problem, we find such rotated frame order by order, using not only J/h but also $h\tau$ as a small parameter.

We first transform the Floquet operator by going to a rotated frame as

$$e^{S}e^{-ih\tau Z}e^{-i\tau H_1}e^{-S} = e^{-ih\tau Z}e^{-i\tau(D+\delta H)}, \tag{4}$$

and demand $[Z, D] = 0$. By appropriately choosing S, D, it will be shown that δH is exponentially small in $\min[O(\frac{h}{J}), O(\frac{1}{h\tau})]$ [71]. Therefore, for small τ and large enough ratio $h/J \gtrsim 0.5$ [70], the operator D approximately commutes with the Floquet unitary in the rotated frame, making $D_{\text{pre}} = e^{-S}De^{S}$ a prethermal quasiconserved observable in the original frame. We emphasize that the right-hand side of Eq. (4) still describes a Floquet system; therefore we derived the quasiconservation without first transforming to a static Hamiltonian. Note that $Z_{\text{pre}} = e^{-S}Ze^{S}$ is quasiconserved in the same sense as D_{pre}. However, whereas D_{pre}, is orthogonal to H_{pre} to zeroth order, $Z_{\text{pre}} \approx H_{\text{pre}} - D_{\text{pre}}$ and it cannot thus be considered an eigenquasiconserved observable.

Now we describe in detail how to find the desired S, D. We first write the transformation given by Eq. (4) in an equivalent form,

$$e^{-i\tau(D+\delta H)} = e^{i\epsilon\tilde{Z}}e^{S}e^{-i\epsilon\tilde{Z}}e^{-i\epsilon^2\tau H_1}e^{-S}. \tag{5}$$

Here we make the shortcut $\tilde{Z} \equiv h\tau Z$, and assume that J/h and $h\tau$ are small parameters of the same order marked by ϵ. S and D can be expressed as a Taylor series of ϵ, $S = \epsilon S_1 + \epsilon^2 S_2 + \cdots, D = \epsilon^2 D_2 + \epsilon^3 D_3 + \cdots$. Because S_j are artificial variables, we can choose S_j such that D_{j+1} satisfy the requirement $[Z, D_{j+1}] = 0$. Repeating the process order by order, we have $[Z, D] = 0$ up to a small error term δH. More specifically, one can do Magnus expansion of the right-hand side of Eq. (5) to get

$$-i\tau\sum_{j=2}^{j^*}\epsilon^j D_j = \sum_{j=2}^{j^*}\epsilon^j([i\tilde{Z}, S_{j-1}] + h_j), \tag{6}$$

where we have ignored the high-order δH. Here, h_j is defined recursively as nest commutators of $i\tilde{Z}$, $-i\tau H_1$ and $S_{j'}$ with $j' < j-1$. For example, the first few orders are

$$\begin{aligned} h_2 &= -i\tau H_1, \\ h_3 &= [S_1, h_2] + \tfrac{1}{2}([i\tilde{Z}, [i\tilde{Z}, S_1]] - [S_1, [S_1, i\tilde{Z}]]). \end{aligned} \tag{7}$$

Recursively, assuming all $S_{j'}$ with $j' < j-1$ (and thus h_j) are known (which is trivially true for $j = 2$), we determine S_{j-1} and D_j from the jth order of Eq. (6) by requiring that $D_j = [i\tilde{Z}, S_{j-1}] + h_j$ commutes with Z. To do this, we first decompose $h_j = \sum_{q=0,\pm1,\cdots} h_{jq}$ such that $[Z, h_{jq}] = qh_{jq}$ (h_{jq} are called the qth quantum coherence of Z [72–74]). This decomposition is possible as long as the dominant part of the Hamiltonian has integer eigenvalues (up to a common constant), a frequent feature shared by the collective rotation $H_2^{(K)} \propto Z$ in our case. $[Z, D] = 0$ is then satisfied by choosing $-i\tau D_j = h_{j0}$ and $S_{j-1} = i\sum_{q\neq0} h_{jq}/(hq\tau)$. We note that S is a sufficiently local operator, $r(S_j) = j$, for KDM with nearest-neighbor interaction. Similar to the prethermal Hamiltonian given by Eq. (3), the expansion in ϵ generally diverges and should be truncated at some order j^*, leading to the exponentially small nonlocal residual δH; see, e.g., Refs. [46,50].

When τ is small, the S_j operators are dominated by the $(J/h)^j$ term. Therefore, in the $\tau \to 0$ limit, the quasiconserved observable found here for the Floquet model reduces to the prethermal quasiconserved observable of the static Hamiltonian $\overline{H}^{(K)}$ [50,70], where the expansion is a series of J/h and $\delta\tilde{H} \approx \exp[-O(h/J)]$. In this regime, $D_{\text{pre}} = -\frac{1}{2}D_z + O[(J/h)^2]$, and the expansion converges for $h/J \gtrsim 0.5$ (up to truncation at exponentially large order) as shown in Ref. [70] (note that here we used $h/J = 1$). Instead, for relatively larger $h\tau$, the S_j operators are dominated by $(h\tau)^j$ and $\delta\tilde{H} \approx \exp[-O(1/h\tau)]$, and thus the system exhibits exponentially slow Floquet heating as expected.

We numerically evaluate the convergence properties of D_{pre} in the KDM [Fig. 4(a)], using the metrics discussed in the previous section, i.e., convergence of the order-by-order expansion terms and infinite-time autocorrelation. We find that the series converges up to order 7 in the $h\tau$ regime that we are interested in. The infinite-time autocorrelation is close to 1 at small τ, as shown in Figs. 4(b) and 4(c), confirming that the local truncation of D_{pre} (as obtained by the first few orders) gives rise to quasiconserved observable $\mathcal{E}_2^{(K)}$. Comparing these results to the prethermal Hamiltonian shown in Figs. 3(b) and 3(c), we find that (i) the normalized autocorrelation of D_{pre} converges to 1 in a larger parameter range ($J\tau \lesssim 1.6$ for D_{pre} and $J\tau \lesssim 1$ for H_{pre}), (ii) the autocorrelation shows a significant drop at $J\tau \gtrsim 1.8$ for D_{pre} and $J\tau \gtrsim 1.2$ for H_{pre}, with a steeper drop when L is increased from 8 to 12. Both facts suggest that D_{pre} is more robust than H_{pre}, in agreement with the experimental results presented in Ref. [51]. This provides evidence that it is possible to realize novel Floquet phases beyond the effective Hamiltonian picture.

IV. TOWARD INFINITE TEMPERATURE: EXPERIMENTAL AND NUMERICAL SIGNATURES

Although it is generally believed that Floquet many-body systems should heat up to infinite temperature, some numerical works [53–56] have found signs of nonthermal behavior in various models. Here we provide evidence of thermalization in the long-time and thermodynamic limit, using numerics and experiments in a NMR quantum simulator [51,70,72], respectively. In simulations, we can access the infinite-time limit using exact diagonalization, but only for small system sizes. Conversely, the system size in NMR experiments is large enough to achieve the thermodynamic limit, but the evolution time cannot be too long due to hardware limitation. Still, by looking at the dynamics for increasingly longer times (experimentally) and larger system sizes (numerically), we can extract insight into the final fate of the Floquet systems.

The experimental system is a single crystal of fluorapatite (FAp) [75]. We study the dynamics of ^{19}F spin-1/2 using NMR techniques. Although the sample is 3D, ^{19}F form a quasi-1D structure because the interaction within the chain is ∼40 times larger than the interaction between different chains [76–78]. The average chain length is estimated to be >50

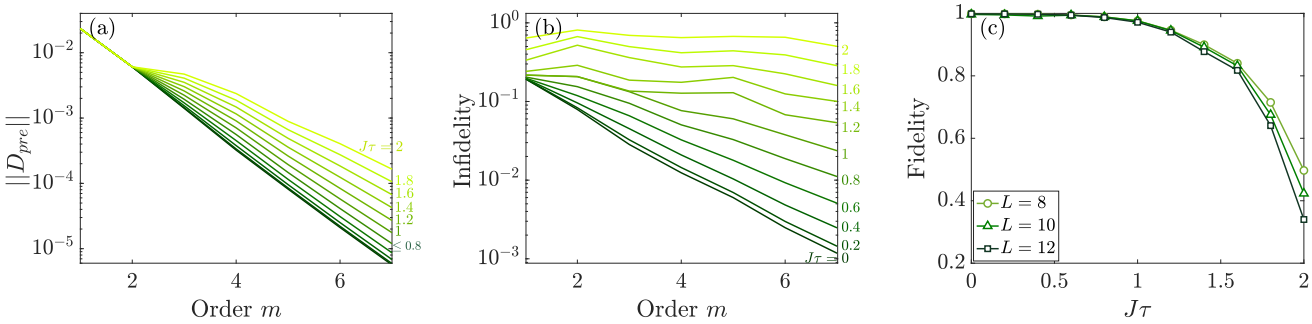

FIG. 4. D_{pre} expansion of KDM. (a) Norm of the mth-order term of the quasiconserved observable D_{pre} (normalized by $L2^L$). Different curves stand for $h\tau = J\tau$ from 0 to 2, in steps of 0.2. The darker color represents smaller $J\tau$. (b) Infidelity $1 - \langle D_{\text{pre}}(\infty) D_{\text{pre}} \rangle$ of infinite-time averaged D_{pre} evaluated up to the mth order. $L = 12$ is used. (c) Fidelity $\langle D_{\text{pre}}(\infty) D_{\text{pre}} \rangle$ evaluated to seventh order as a function of $h\tau$ for different system sizes.

and the coherence time of the ^{19}F spins is $T_1 \approx 0.8$ s. The sample is placed in a 7 T magnetic field where the Zeeman interaction dominates, thus reducing the ^{19}F spins interaction to the secular dipolar Hamiltonian $H = J_0 D_z$ with $J_0 = -29.7$ krad/s (we define z as the magnetic field direction). While the corresponding 1D, nearest-neighbor XXZ Hamiltonian is integrable [79–81], the experimental $1/r^3$ Hamiltonian can lead to diffusive [82,83] and chaotic [84] behavior in 3D. In the presence of a transverse field, the system is known to show a quantum phase transition [85]. We use 16 rf pulses [51,70,72,86] to engineer the natural Hamiltonian into $H_1^{(A)} = JD_y$ and $H_2^{(A)} = JD_x$ with tunable J. This enables varying the Floquet steps by tuning J, while keeping τ fixed. Then, experimental imperfections such as decoherence and pulse errors remain the same, and we can faithfully quantify the Floquet heating rate. The initial state is a high-temperature thermal state with small thermal polarization in the magnetic field direction, $\rho(0) \approx (\mathbb{1} - \epsilon Z)/2^L$ with $\epsilon \approx 10^{-5}$, and the observable is the collective magnetization along the x axis, $\mathcal{O} = X$. As the identity part does not change under unitary evolution and does not contribute to the signal, it is convenient to consider only the deviation from the identity $\delta\rho(0) = Z$, which can be rotated to a desired observable $\mathcal{O}'$. Therefore, the NMR signal is equivalent to an infinite-temperature correlation, $\text{Tr}[\delta\rho(t)X] \to \langle \mathcal{O}'(t)\mathcal{O} \rangle_{\beta=0}$.

We experimentally study the heating rates of the quasiconserved observables and their scaling with Floquet period to reveal the prethermal phase and investigate the eventual heating to infinite temperature. In Fig. 5, we show results for ADM (the two quasiconserved observables in KDM show similar behavior as reported elsewhere [51]). To study the autocorrelation of $H_{\text{pre}} = \overline{H} + O(\tau)$ in ADM, we measure the average Hamiltonian, $\overline{H}^{(A)} = JD_y + JD_x = -JD_z$, since the higher-order terms in Eq. (3) are not accessible. We use the Jeener-Broekaert pulse pair [87] to evolve the initial state $\delta\rho$ and experimental observable X into $D_z \propto \overline{H}^{(A)}$. Because of the difference $H_{\text{pre}} - \overline{H}$, we still expect an initial transient, over a time $\sim \|H_{\text{pre}}\|^{-1}$, where the average Hamiltonian thermalizes to the prethermal Hamiltonian. When more Floquet periods are applied, the autocorrelation of D_z slowly decays from its prethermal value.

The decay rate in the prethermalization regime is shown in Fig. 5(b) and can be fitted to an exponential function in $1/(J\tau)$ on top of a constant background decay (which is due to experimental imperfections; see SM [88] for more details). By normalizing the data to the data collected under the fastest drive ($J\tau = 0.35$), the background decay is canceled, and the resulting dynamics only arises from the coherent evolution, as shown in Fig. 5(c). For given n, the normalized correlation decreases when increasing $J\tau$ because $H_{\text{pre}} = \overline{H} + O(J\tau)$ and thus $\overline{H}$ that we measure has less overlap with the true quasiconserved observable H_{pre} for larger $J\tau$. The overall drop of the curves when increasing n is instead an indicator of Floquet heating.

To better quantify the final thermalization process, we define a critical value J_c such that when $J\tau > J_c\tau$, the system is thermalized at a given number n of periods in the thermodynamic limit or for a system size L at infinite time. Studying the scaling of J_c as a function of n (experimentally) and L (numerically) provides hints on the long-time, thermodynamic limits.

We numerically obtain the autocorrelations $\langle \mathcal{O}(\infty)\mathcal{O} \rangle$ as a function of $J\tau$ using exact diagonalization. In Fig. 6(a), we show simulation results for $\mathcal{O} = \overline{H}^{(K)}, D_z$ for KDM, and $\mathcal{O} = \overline{H}^{(A)}$ for ADM. (Here we explicitly consider the exact dipolar interaction instead of truncating to nearest neighbors). Note that both observables in KDM show a nonmonotonic behavior. They appear to be quasiconserved until $J\tau = 1$; the decrease in overlap is, however, interrupted by a revival at $J\tau = 1.6$. This is because $\overline{H}^{(K)}$ and D_z are an approximation of H_{pre} and D_{pre} to leading order. Thus, $\overline{H}^{(K)}$ (D_z) still has a small overlap with D_{pre} (H_{pre}), giving rise to a second plateau at $J\tau \approx 1.6$ ($J\tau \approx 1$). The experimentally measured autocorrelations of quasiconserved observables in KDM can be found in [51]. For both experiments and simulations, we then find $J_c\tau$ from the point where the curves drop below a threshold value of 0.5 (any other reasonable choice would not qualitatively change the results). We linearly interpolate between data points to get $J_c\tau$ for every quasiconserved observable and plot the $J_c\tau$ in Figs. 6(b) and 6(c). The decrease of numerically calculated $J_c\tau$ with L in Fig. 6(b) indicates that even the correlations of quasiconserved observables decay to zero

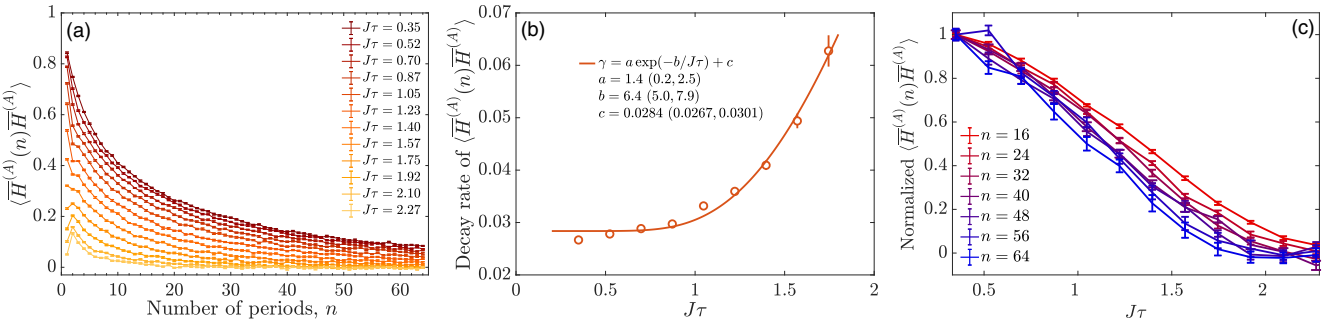

FIG. 5. Autocorrelation of the average Hamiltonian for the alternating dipolar model. (a) Autocorrelation as a function of n. Different curve stands for $J\tau$ from 0.35 to 2.27, with a step of 0.175. The darker color represents smaller $J\tau$ and the lighter color represents larger $J\tau$. We fit the autocorrelations from $n = 20$ to $n = 64$ to exponentially decaying function $\exp(-\gamma n)$ and plot the decay rate γ in (b). The length of the error bars corresponds to two standard deviations of the fitted decay rate. The solid curve indicates the fit to function $\gamma = a\exp(-b/J\tau) + c$. The fitted coefficients a, b, c are shown in the plot with the 95% confidence interval. (c) Autocorrelation vs $J\tau$ for different n. The lighter colors represent smaller n and the darker colors represent larger n. For a given n, the autocorrelation is normalized by $\langle \overline{H}(n)\overline{H} \rangle$ at $J\tau = 0.35$, i.e., the leftmost point is normalized to 1. In (a) and (b), error bars are determined from the noise in the free induction decay [see the Supplemental Material (SM) [88] for details of the experimental scheme].

as the system thermalizes to infinite temperature, suggesting that this nonthermalizing behavior should not persist to the thermodynamic limit. A similar result is also observed from experimentally measured $J_c\tau$, as shown in Fig. 6(c) [89]. Note that although $J_c\tau$ for $\langle \overline{H}^{(K)}(n)\overline{H}^{(K)} \rangle$ shows only a moderate dependence on n [Fig. 6(c)], its decay is still larger than experimental uncertainties.

V. CONCLUSION

As Floquet driving is a promising avenue for quantum simulation, it is crucial to evaluate its robustness, the existence of a long-lived prethermal phase, and the eventual thermalization to infinite temperature. Investigating Floquet heating, which breaks the prethermal regime, is particularly challenging, not only because of inherent limitations in numerical and experimental studies, but also because of the challenge to properly identify all quasiconserved observables in the complex, many-body driven dynamics.

Here we tackle both of these issues by combining analytical, numerical, and experimental tools. First, we provide a systematic strategy to find local, eigenquasiconserved observables in the prethermal regime using infinite-temperature correlations. By systematically searching over local operators, we find that counterintuitive quasiconserved observables might emerge, as we identify two eigenquasiconserved observables: the first, not surprisingly, is associate with energy, H_{pre}, under sufficient fast drive; in addition, we find another quasiconserved observable, D_{pre}, for the KDM in the presence of a large driving field. Our search protocol would be useful in other settings, such as identifying the underlying Hamiltonian or symmetries from measurements.

We then use numerical and experimental evidence to obtain insight into the inaccessible thermodynamic limit and long-time regime, to show that autocorrelations of quasiconserved observables indeed decrease toward zero due to Floquet heating, suggesting the Floquet system approaches the infinite-temperature state.

Our results not only provide a metric to study thermalization in driven quantum systems, but also open intriguing perspectives into the existence of quasiconserved observ-

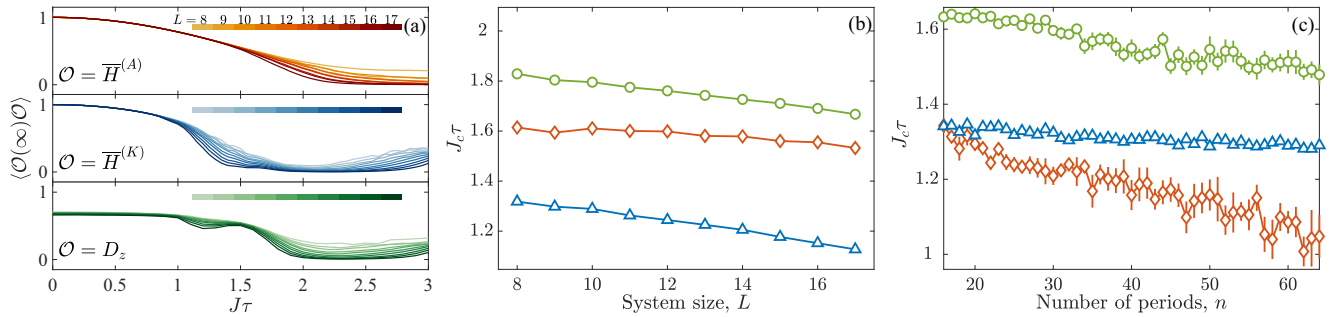

FIG. 6. Scaling of the critical Trotter step for KDM ($\overline{H}^{(K)}$: blue; D_z: green) and ADM ($\overline{H}^{(A)}$: red). (a) Simulated autocorrelations as a function of $J\tau$ for $L = 8, 9, \ldots, 17$ using exact diagonalization. The darker colors represent larger L as shown in the color bar. (b) $J_c\tau$ at which the numerical autocorrelation ($L = 17$) drops to half of the value under infinitely fast driving ($J\tau \to 0$). (c) $J_c\tau$ at which the experimentally measured autocorrelation drops to half of the value under the fastest driving ($J\tau = 0.35$). Error bars are determined from the noise in the free induction decay (see SM [88]).

ables other than the energy. It is an open question when they emerge and how they interact with each other. A better understanding of quasiconserved observables would benefit our understanding of heating in closed driven systems and in designing a robust protocol to slow down thermalization.

ACKNOWLEDGMENTS

The authors would like to thank H. Zhou, W.-J Zhang, and Z. Li for discussion. This work was supported in part by the National Science Foundation under Grants No. PHY1734011, No. PHY1915218, and No. OIA-1921199.

[1] A. Eckardt, C. Weiss, and M. Holthaus, Phys. Rev. Lett. **95**, 260404 (2005).
[2] N. Tsuji, T. Oka, P. Werner, and H. Aoki, Phys. Rev. Lett. **106**, 236401 (2011).
[3] J. Mentink, K. Balzer, and M. Eckstein, Nat. Commun. **6**, 6708 (2015).
[4] S. Kitamura and H. Aoki, Phys. Rev. B **94**, 174503 (2016).
[5] R. Mikhaylovskiy, E. Hendry, A. Secchi, J. H. Mentink, M. Eckstein, A. Wu, R. Pisarev, V. Kruglyak, M. Katsnelson, T. Rasing *et al.*, Nat. Commun. **6**, 8190 (2015).
[6] F. Görg, M. Messer, K. Sandholzer, G. Jotzu, R. Desbuquois, and T. Esslinger, Nature (London) **553**, 481 (2018).
[7] N. H. Lindner, G. Refael, and V. Galitski, Nat. Phys. **7**, 490 (2011).
[8] Y. Wang, H. Steinberg, P. Jarillo-Herrero, and N. Gedik, Science **342**, 453 (2013).
[9] T. Oka and H. Aoki, Phys. Rev. B **79**, 081406(R) (2009).
[10] Z. Gu, H. A. Fertig, D. P. Arovas, and A. Auerbach, Phys. Rev. Lett. **107**, 216601 (2011).
[11] A. G. Grushin, A. Gómez-León, and T. Neupert, Phys. Rev. Lett. **112**, 156801 (2014).
[12] L. E. F. Foa Torres, P. M. Perez-Piskunow, C. A. Balseiro, and G. Usaj, Phys. Rev. Lett. **113**, 266801 (2014).
[13] M. S. Rudner, N. H. Lindner, E. Berg, and M. Levin, Phys. Rev. X **3**, 031005 (2013).
[14] L. Jiang, T. Kitagawa, J. Alicea, A. R. Akhmerov, D. Pekker, G. Refael, J. I. Cirac, E. Demler, M. D. Lukin, and P. Zoller, Phys. Rev. Lett. **106**, 220402 (2011).
[15] A. Kundu and B. Seradjeh, Phys. Rev. Lett. **111**, 136402 (2013).
[16] T. Kitagawa, E. Berg, M. Rudner, and E. Demler, Phys. Rev. B **82**, 235114 (2010).
[17] D. V. Else, P. Fendley, J. Kemp, and C. Nayak, Phys. Rev. X **7**, 041062 (2017).
[18] N. Goldman and J. Dalibard, Phys. Rev. X **4**, 031027 (2014).
[19] M. Bukov, L. D'Alessio, and A. Polkovnikov, Adv. Phys. **64**, 139 (2015).
[20] M. Bukov, M. Kolodrubetz, and A. Polkovnikov, Phys. Rev. Lett. **116**, 125301 (2016).
[21] J. Struck, C. Ölschläger, M. Weinberg, P. Hauke, J. Simonet, A. Eckardt, M. Lewenstein, K. Sengstock, and P. Windpassinger, Phys. Rev. Lett. **108**, 225304 (2012).
[22] M. Aidelsburger, M. Atala, M. Lohse, J. T. Barreiro, B. Paredes, and I. Bloch, Phys. Rev. Lett. **111**, 185301 (2013).
[23] J. Struck, J. Simonet, and K. Sengstock, Phys. Rev. A **90**, 031601(R) (2014).
[24] H. F. Trotter, Proc. Am. Math. Soc. **10**, 545 (1959).
[25] S. Lloyd, Science **273**, 1073 (1996).
[26] Y.-X. Liu, J. Hines, Z. Li, A. Ajoy, and P. Cappellaro, Phys. Rev. A **102**, 010601(R) (2020).
[27] G. Jotzu, M. Messer, R. Desbuquois, M. Lebrat, T. Uehlinger, D. Greif, and T. Esslinger, Nature (London) **515**, 237 (2014).
[28] M. Aidelsburger, M. Lohse, C. Schweizer, M. Atala, J. T. Barreiro, S. Nascimbene, N. R. Cooper, I. Bloch, and N. Goldman, Nat. Phys. **11**, 162 (2015).
[29] C. Kokail, C. Maier, R. van Bijnen, T. Brydges, M. Joshi, P. Jurcevic, C. Muschik, P. Silvi, R. Blatt, C. Roos *et al.*, Nature (London) **569**, 355 (2019).
[30] A. M. Childs, D. Maslov, Y. Nam, N. J. Ross, and Y. Su, Proc. Natl. Acad. Sci. USA **115**, 9456 (2018).
[31] S. Choi, J. Choi, R. Landig, G. Kucsko, H. Zhou, J. Isoya, F. Jelezko, S. Onoda, H. Sumiya, V. Khemani, C. von Keyserlingk, N. Y. Yao, E. Demler, and M. D. Lukin, Nature (London) **543**, 221 (2017).
[32] J. Zhang, P. W. Hess, A. Kyprianidis, P. Becker, A. Lee, J. Smith, G. Pagano, I.-D. Potirniche, A. C. Potter, A. Vishwanath, N. Y. Yao, and C. Monroe, Nature (London) **543**, 217 (2017).
[33] R. Moessner and S. L. Sondhi, Nat. Phys. **13**, 424 (2017).
[34] D. J. Luitz, R. Moessner, S. L. Sondhi, and V. Khemani, Phys. Rev. X **10**, 021046 (2020).
[35] F. Machado, D. V. Else, G. D. Kahanamoku-Meyer, C. Nayak, and N. Y. Yao, Phys. Rev. X **10**, 011043 (2020).
[36] D. H. Dunlap and V. M. Kenkre, Phys. Rev. B **34**, 3625 (1986).
[37] S. Fishman, D. R. Grempel, and R. E. Prange, Phys. Rev. Lett. **49**, 509 (1982).
[38] V. M. Bastidas, C. Emary, B. Regler, and T. Brandes, Phys. Rev. Lett. **108**, 043003 (2012).
[39] V. M. Bastidas, C. Emary, G. Schaller, and T. Brandes, Phys. Rev. A **86**, 063627 (2012).
[40] F. Großmann, T. Dittrich, P. Jung, and P. Hänggi, Phys. Rev. Lett. **67**, 516 (1991).
[41] F. Großmann and P. Hänggi, Europhys. Lett. **18**, 571 (1992).
[42] M. Grifoni and P. Hänggi, Phys. Rep. **304**, 229 (1998).
[43] A. Lazarides, A. Das, and R. Moessner, Phys. Rev. E **90**, 012110 (2014).
[44] L. D'Alessio and M. Rigol, Phys. Rev. X **4**, 041048 (2014).
[45] H. Kim, T. N. Ikeda, and D. A. Huse, Phys. Rev. E **90**, 052105 (2014).
[46] D. A. Abanin, W. De Roeck, W. W. Ho, and F. Huveneers, Phys. Rev. B **95**, 014112 (2017).
[47] D. A. Abanin, W. De Roeck, and F. Huveneers, Phys. Rev. Lett. **115**, 256803 (2015).
[48] T. Kuwahara, T. Mori, and K. Saito, Ann. Phys. **367**, 96 (2016).
[49] D. Abanin, W. De Roeck, W. W. Ho, and F. Huveneers, Commun. Math. Phys. **354**, 809 (2017).
[50] D. V. Else, B. Bauer, and C. Nayak, Phys. Rev. X **7**, 011026 (2017).
[51] P. Peng, C. Yin, X. Huang, C. Ramanathan, and P. Cappellaro, Nat. Phys. (2021), doi: 10.1038/s41567-020-01120-z.

[52] A. Rubio-Abadal, M. Ippoliti, S. Hollerith, D. Wei, J. Rui, S. L. Sondhi, V. Khemani, C. Gross, and I. Bloch, Phys. Rev. X **10**, 021044 (2020).

[53] M. Heyl, P. Hauke, and P. Zoller, Sci. Adv. **5**, eaau8342 (2019).

[54] L. D'Alessio and A. Polkovnikov, Ann. Phys. **333**, 19 (2013).

[55] L. M. Sieberer, T. Olsacher, A. Elben, M. Heyl, P. Hauke, F. Haake, and P. Zoller, npj Quantum Inf. **5**, 78 (2019).

[56] T. Prosen, Phys. Rev. E **60**, 3949 (1999).

[57] D. A. Abanin, W. De Roeck, and F. Huveneers, Ann. Phys. **372**, 1 (2016).

[58] A. Lazarides, A. Das, and R. Moessner, Phys. Rev. Lett. **115**, 030402 (2015).

[59] P. Ponte, Z. Papić, F. Huveneers, and D. A. Abanin, Phys. Rev. Lett. **114**, 140401 (2015).

[60] L. Zhang, V. Khemani, and D. A. Huse, Phys. Rev. B **94**, 224202 (2016).

[61] H. C. Po, L. Fidkowski, T. Morimoto, A. C. Potter, and A. Vishwanath, Phys. Rev. X **6**, 041070 (2016).

[62] P. Bordia, H. Lüschen, U. Schneider, M. Knap, and I. Bloch, Nat. Phys. **13**, 460 (2017).

[63] V. Khemani, A. Lazarides, R. Moessner, and S. L. Sondhi, Phys. Rev. Lett. **116**, 250401 (2016).

[64] K. Ji and B. V. Fine, Phys. Rev. Lett. **121**, 050602 (2018).

[65] T. Prosen, Phys. Rev. Lett. **80**, 1808 (1998).

[66] In the following, we drop the subscript $\beta = 0$ for simplicity.

[67] P. Mazur, Physica **43**, 533 (1969).

[68] W. Magnus, Commun. Pure Appl. Math. **7**, 649 (1954).

[69] S. Blanes, F. Casas, J. Oteo, and J. Ros, Phys. Rep. **470**, 151 (2009).

[70] K. X. Wei, P. Peng, O. Shtanko, I. Marvian, S. Lloyd, C. Ramanathan, and P. Cappellaro, Phys. Rev. Lett. **123**, 090605 (2019).

[71] Note that the matrix representation of Z' ($\tilde{Z}$) in the frame transformed by $e^{S'}$ (e^{S}) is the same as that of Z in the original frame, so they are different physical quantities.

[72] K. X. Wei, C. Ramanathan, and P. Cappellaro, Phys. Rev. Lett. **120**, 070501 (2018).

[73] M. Munowitz and A. Pines, in *Principle and Applications of Multiple-Quantum NMR*, Advances in Chemical Physics, edited by I. Prigogine and S. Rice (Wiley, New York, 1975).

[74] M. Gärttner, P. Hauke, and A. M. Rey, Phys. Rev. Lett. **120**, 040402 (2018).

[75] W. V. der Lugt and W. Caspers, Physica **30**, 1658 (1964).

[76] P. Cappellaro, C. Ramanathan, and D. G. Cory, Phys. Rev. Lett. **99**, 250506 (2007).

[77] W. Zhang, P. Cappellaro, N. Antler, B. Pepper, D. G. Cory, V. V. Dobrovitski, C. Ramanathan, and L. Viola, Phys. Rev. A **80**, 052323 (2009).

[78] C. Ramanathan, P. Cappellaro, L. Viola, and D. G. Cory, New J. Phys. **13**, 103015 (2011).

[79] F. C. Alcaraz, M. N. Barber, M. T. Batchelor, R. J. Baxter, and G. R. W. Quispel, J. Phys. A: Math. Gen. **20**, 6397 (1987).

[80] E. K. Sklyanin, J. Phys. A: Math. Gen. **21**, 2375 (1988).

[81] Y. Wang, W.-L. Yang, J. Cao, and K. Shi, *Off-Diagonal Bethe Ansatz for Exactly Solvable Models* (Springer, New York, 2016).

[82] D. K. Sodickson and J. S. Waugh, Phys. Rev. B **52**, 6467 (1995).

[83] W. Zhang and D. G. Cory, Phys. Rev. Lett. **80**, 1324 (1998).

[84] D. Jyoti, arXiv:1711.01948.

[85] A. Isidori, A. Ruppel, A. Kreisel, P. Kopietz, A. Mai, and R. M. Noack, Phys. Rev. B **84**, 184417 (2011).

[86] C. M. Sánchez, A. K. Chattah, K. X. Wei, L. Buljubasich, P. Cappellaro, and H. M. Pastawski, Phys. Rev. Lett. **124**, 030601 (2020).

[87] J. Jeener and P. Broekaert, Phys. Rev. **157**, 232 (1967).

[88] See Supplemental Material at http://link.aps.org/supplemental/10.1103/PhysRevB.103.054305 for experimental system and error analysis.

[89] We note that discrepancies in the value of $J_c\tau$ and order of curves in Figs. 6(a) and 6(c) are to be expected because, although $J_c\tau$ approaches zero when $L \to \infty$ and $n \to \infty$, the convergence speed depends on the path to that limit.

Prethermal quasiconserved observables in Floquet quantum systems

Chao Yin,[1,*] Pai Peng (),[2,†] Xiaoyang Huang,[1] Chandrasekhar Ramanathan,[3] and Paola Cappellaro[4,1,‡]

[1] *Research Laboratory of Electronics, Massachusetts Institute of Technology, Cambridge, Massachusetts 02139, USA*
[2] *Department of Electrical Engineering and Computer Science, Massachusetts Institute of Technology, Cambridge, MA 02139*
[3] *Department of Physics and Astronomy, Dartmouth College, Hanover, NH 03755, USA*
[4] *Department of Nuclear Science and Engineering, Massachusetts Institute of Technology, Cambridge, MA 02139*

(Dated: February 5, 2021)

I. EXPERIMENTAL BACKGROUND DECAY RATE AS A FUNCTION OF $J\tau$

In the main text we measured the Floquet heating for a periodic, Hamiltonian switching scheme. While it would be easy to change the period by increasing the time between switches, this would lead to experiments performed with different total times or a different number of control operations. In turns, this can introduce variable amount of decoherence and relaxation effects, and of control errors. Instead, we kept the time for one Floquet period constant and used Hamiltonian engineering to vary the Hamiltonian strength in order to vary the Floquet driving frequency.

One of the assumptions in our work is that the background decay rate does not change much with driving frequency (compared to the change in Floquet heating rate). In this section, we provide experimental evidence for this assertion. When changing driving frequency, we are changing (i) the effective strength J of the engineered dipolar interaction JD_y and (ii) the kicking angle in the kicked dipolar model by a phase shift (see II C). As phase shift angles are usually very accurately implemented in NMR experiments, we focus on the engineered dipolar interaction, which is obtained by Floquet engineering itself, as explained in II C. To quantify how good is the engineered JD_y, we measure $\langle Y(n)Y\rangle$ and $\langle D_y(n)D_y\rangle$ under the engineered Hamiltonian JD_y, without kicking field nor direction alternation, as shown in Fig. S1.

Note that the maximum difference between the decay rate of $\langle D_y(n)D_y\rangle$ over the range of $J\tau$ considered is ~ 0.003, much smaller than the Floquet heating rate in the main text. A quantitative analysis is challenging because the specific form of error terms is unknown, and JD_y is an interacting Hamiltonian thus error accumulation is intractable. Here we use some simple arguments to argue that variations in the background decay with $J\tau$ have little to no influence on our results. First, we note that while in the main text we are interested in

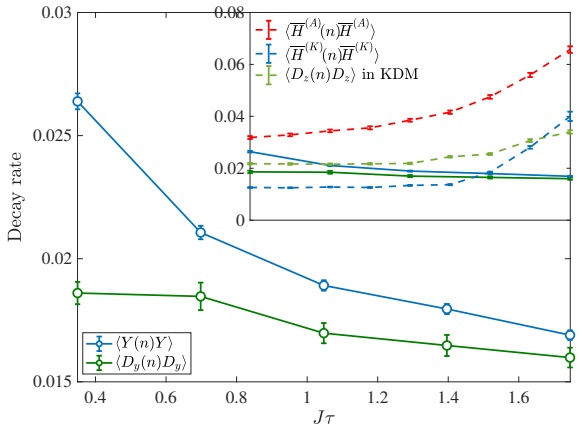

FIG. S1. Decay rate of $\langle Y(n)Y\rangle$ (blue) and $\langle D_y(n)D_y\rangle$ (green) under engineered dipolar Hamiltonian JD_y as a function of $J\tau$. The range of $J\tau$ studied was obtained by varying the scaling u (see SM [S1]) from 0.098 to 0.646, while keeping fixed $\tau = 120\mu s$. In the inset, we compare the background decay rates with the Floquet decay rates (dashed lines).

the decay of the autocorrelation of H_{pre} and D_{pre}, here with $H = JDy$ we can only discuss the decay of D_y and Y, since other observables that are not conserved display very fast decay which is not informative. For example, in the main text we measure D_z, which thermalizes even under the ideal D_y and thus we cannot distinguish thermalization from decay due to experimental imperfections in the engineered dipolar Hamiltonian D_y. Still, as D_z and D_y overlap, if the background decay of D_z had a significant change with $J\tau$, it would be reflected in D_y, which is not observed. Therefore, we expect the change in the background decay rate for $\langle D_z(n)D_z\rangle$ to be small as well. Here we can only probe the background decay rate of Y, while in the main text we are interested in the longitudinal magnetization, Z, that appears in $\langle \overline{H}^{(K)}(n)\overline{H}^{(K)}\rangle$ [see Fig. 6(c) in the main text]. The transverse magnetization decay rate is, however, a upper bound for Z, since in NMR experiments Z is usually more robust against errors than Y due to the large magnetic field in z-axis that suppresses decoherence and experimental errors that do

* yinchao1998@pku.edu.cn
† C.Y. and P.P. contributed equally to this work.
‡ pcappell@mit.edu

not conserve the total Zeeman energy (we note that we typically do not explicitly write the Zeeman energy in the Hamiltonians as we work in the rotating frame). Even if the variation in the background decay for Z were as large as what observed for Y in these experiments (~ 0.009), it would still be still small compared with Floquet (see inset of Fig. S1). In addition, in the kicked dipolar model, we can consider D_y as being subjected to rotations along Z that further cancel out the error terms in the engineered JD_y that do not conserve Z. As a result, the decay rate of Y due to the engineered D_y is larger, by about a factor of 2, than the baseline decay of $\langle \overline{H}^{(K)}(n)\overline{H}^{(K)}\rangle$ in the kicked dipolar model (they are 0.254 and 0.123, respectively, in the fastest driving case $J\tau = 0.35$).

II. EXPERIMENTAL SYSTEM, CONTROL AND DATA ANALYSIS

A. Experimental System

The system used in the experiment was a single crystal of fluorapatite (FAp). Fluorapatite is a hexagonal mineral with space group $P6_3/m$, with the ^{19}F spin-1/2 nuclei forming linear chains along the c-axis. Each fluorine spin in the chain is surrounded by three ^{31}P spin-1/2 nuclei. We used a natural crystal, from which we cut a sample of approximate dimensions 3 mm×3 mm×2 mm. The sample is placed at room temperature inside an NMR superconducting magnet producing a uniform $B = 7$ T field. The total Hamiltonian of the system is given by

$$H_{\rm tot} = \omega_F \sum_k S_z^k + \omega_P \sum_\kappa s_z^\kappa + H_F + H_P + H_{FP} \quad \text{(S1)}$$

The first two terms represent the Zeeman interactions of the F(S) and P(s) spins, respectively, with frequencies $\omega_F = \gamma_F B \approx (2\pi)282.37$ MHz and $\omega_P = \gamma_P B = (2\pi)121.51$ MHz, where $\gamma_{F/P}$ are the gyromagnetic ratios. The other three terms represent the natural magnetic dipole-dipole interaction among the spins, given generally by

$$H_{\rm dip} = \sum_{j<k} \frac{\hbar\gamma_j\gamma_k}{|\vec{r}_{jk}|^3}\left[\vec{S}_j\cdot\vec{S}_k - \frac{3\vec{S}_j\cdot\vec{r}_{jk}\,\vec{S}_k\cdot\vec{r}_{jk}}{|\vec{r}_{jk}|^2}\right], \quad \text{(S2)}$$

where $\vec{r}_{ij}$ is the vector between the ij spin pair. Because of the much larger Zeeman interaction, we can truncate the dipolar Hamiltonian to its energy-conserving part (secular Hamiltonian). We then obtain the homonuclear Hamiltonians

$$\begin{aligned} H_F &= \frac{1}{2}\sum_{j<k} J_{jk}^F(2S_z^jS_z^k - S_x^jS_x^k - S_y^jS_y^k) \\ H_P &= \frac{1}{2}\sum_{\lambda<\kappa} J_{\kappa\lambda}^P(2s_z^\lambda s_z^\kappa - s_x^\lambda s_x^\kappa - s_y^\lambda s_y^\kappa) \end{aligned} \quad \text{(S3)}$$

and the heteronuclear interaction between the F and P spins,

$$H_{FP} = \sum_{k,\kappa} J_{k,\kappa}^{FP} S_z^k s_z^\kappa, \quad \text{(S4)}$$

with $J_{jk} = \hbar\gamma_j\gamma_k\frac{1-3\cos(\theta_{jk})^2}{|\vec{r}_{jk}|^3}$, where θ_{jk} is the angle between the vector $\vec{r}_{jk}$ and the magnetic field z-axis. The maximum values of the couplings (for the closest spins) are given respectively by $J^F = -32.76$ krad s^{-1}, $J^P = 1.20$ krad s^{-1} and $J^{FP} = 6.12$ krad s^{-1}.

The dynamics of this complex many-body system can be mapped to a much simpler, quasi-1D system. First, we note that when the crystal is oriented with its c-axis parallel to the external magnetic field the coupling of fluorine spins to the closest off-chain fluorine spin is ≈ 40 times weaker, while in-chain, next-nearest neighbor couplings are 8 times weaker. Previous studies on these crystals have indeed observed dynamics consistent with spin chain models, and the system has been proposed as solid-state realizations of quantum wires [S2–S4]. This approximation of the experimental system to a 1D, short-range system, although not perfect has been shown to reliably describe experiments for relevant time-scales [S5, S6]. The approximation breaks down at longer times, with a convergence of various effects: long-range in-chain and cross-chain couplings, as well as pulse errors in the sequences used for Hamiltonian engineering. In addition, the system also undergoes spin relaxation, although on a much longer time-scale ($T_1 = 0.8$ s for our sample).

B. Error analysis

In experiments, we want to measure the correlation $\langle\delta\rho(t)\mathcal{O}\rangle$, where $\delta\rho(t) = U(t)\delta\rho(0)U(t)$ is the nontrivial part of the density matrix evolved under a pulse-control sequence for a time t. Instead of just performing a single measurement after the sequence, we continuously monitor the free evolution of $\delta\rho(t)$ under the natural Hamiltonian $H_{\rm dip}$, from t to $t + t_{\rm FID}$. The measured signal is called in NMR free induction decay (FID) and a typical FID trace is shown in Fig. S3). This signal trace allows us to extract not only the amplitude of the correlation

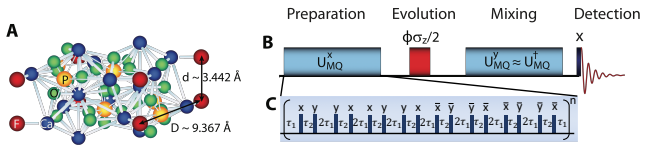

FIG. S2. **A** Fluorapatite crystal structure, showing the Fluorine and Phosphorus spins in the unit cell. **B** NMR scheme for the generation and detection of MQC. In the inset (**C**) an exemplary pulse sequence for the generation of the $H_{\rm dipy}$. Note that thanks to the ability of inverting the sign of the Hamiltonian, the scheme amounts to measuring out-of-time order correlations.

(from the first data point) but also its uncertainty. We take the standard deviation of the last 20 data points in the FID as the uncertainty of the $\langle \delta\rho(t)\mathcal{O}\rangle$. This uncertainty is used with linear error propagation to obtain the error bars of all the quantities analyzed in the main text.

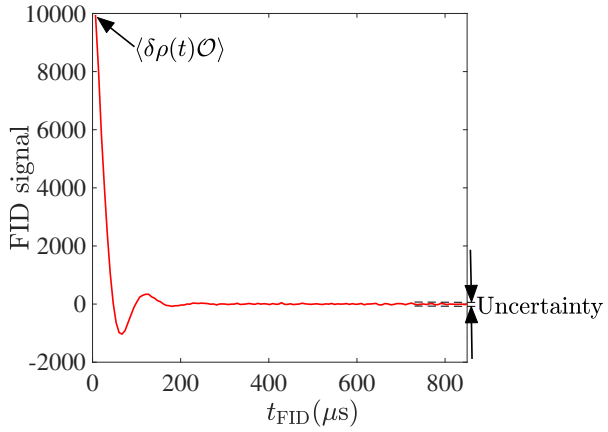

FIG. S3. An example of FID. 128 data points are taken in total. The first data point gives $\langle(\delta\rho(t)\mathcal{O}\rangle$ and the standard deviation of the last 20 points gives the uncertainty of $\langle(\delta\rho(t)\mathcal{O}\rangle$.

C. Hamiltonian Engineering

In the main text we focused on the Floquet heating (Trotter error) for a periodic alternating scheme, switching between two Hamiltonians. In order to avoid longer times and/or different numbers of control operations when changing the Trotter step (Floquet period), we engineered Hamiltonians of variable strengths. Then, the Hamiltonians themselves are obtained stroboscopically by applying periodic rf pulse trains to the natural dipolar Hamiltonian that describes the system, and are thus themselves Floquet Hamiltonians. Since we only varied the sequences, but not the Floquet period, this step does not contribute to the behavior described in the main text, as we further investigate in I.

We used Average Hamiltonian Theory (AHT [S7]) as the basis for our Hamiltonian engineering method, to design the control sequences and determine the approximation errors. The dynamics is induced by the total Hamiltonian $H = H_{\mathrm{dip}} + H_{\mathrm{rf}}$, where $H_{\mathrm{dip}} = \frac{1}{2}\sum_{j<k} J_{jk}(2S_z^jS_z^k - S_x^jS_x^k - S_y^jS_y^k) + \sum_j h_jS_z^j$ is the system Hamiltonian, and $H_{\mathrm{rf}}(t)$ is the external Hamiltonian due to the rf-pulses. The density matrix ρ evolves under the total Hamiltonian according to $\dot{\rho} = -i[H,\rho]$. We study the dynamics into a convenient interaction frame, defined by $\rho' = {U_{\mathrm{rf}}}^{\dagger}\rho U_{\mathrm{rf}}$, where $U_{\mathrm{rf}}(t) = \mathcal{T}\exp[-i\int_0^t H_{\mathrm{rf}}(t')dt']$ and $\mathcal{T}$ is the time ordering operator. In this *toggling* frame, ρ' evolves according to $\dot{\rho}' = -i[H(t),\rho']$, where $H(t) = {U_{\mathrm{rf}}}^{\dagger}H_{\mathrm{dip}}U_{\mathrm{rf}}$. Since U_{rf} is periodic, $H(t)$ is also periodic with the same period τ, and gives rise to the Floquet Hamiltonian, H_F, as as $U(\tau) = \exp[-iH_F\tau]$. Note that if the pulse sequence satisfies the condition $U_{\mathrm{rf}}(\tau) = 1$, the dynamics of ρ and ρ' are identical when the system is viewed stroboscopically, i.e., at integer multiples of τ, where the toggling frame coincides with the (rotating) lab frame.

We devised control sequences to engineer a scale-down, rotated version of the dipolar Hamiltonian [S8, S9]. We usually look for control sequences that would engineer the desired Hamiltonian up to second order in the Magnus-Floquet expansion. Then, to engineer the interaction D_y, we use a 16-pulse sequence. The basic building block is given by a 4-pulse sequence [S10, S11] originally developed to study MQC. We denote a generic 4-pulse sequence as $P(\tau_1,\mathbf{n}_1,\tau_2,\mathbf{n}_2,\tau_3,\mathbf{n}_3,\tau_4,\mathbf{n}_4,\tau_5)$, where $\mathbf{n}_j$ represents the direction of the j-th $\pi/2$ pulse, and τ_j's the delays interleaving the pulses. In our experiments, the $\pi/2$ pulses have a width t_w of typically 1 μs. τ_j starts and/or ends at the midpoints of the pulses (see also Fig. S2). In this notation, our forward 16-pulse sequence can be expressed as

$$P(\tau_1,\mathbf{x},\tau_2,\mathbf{y},2\tau_1,\mathbf{y},\tau_2,\mathbf{x},\tau_1)P(\tau_1,\mathbf{x},\tau_2,\mathbf{y},2\tau_1,\mathbf{y},\tau_2,\mathbf{x},\tau_1)P(\tau_1,\overline{\mathbf{x}},\tau_2,\overline{\mathbf{y}},2\tau_1,\overline{\mathbf{y}},\tau_2,\overline{\mathbf{x}},\tau_1)P(\tau_1,\overline{\mathbf{x}},\tau_2,\overline{\mathbf{y}},2\tau_1,\overline{\mathbf{y}},\tau_2,\overline{\mathbf{x}},\tau_1)$$

and the backward sequence as

$$P(\tau_3,\mathbf{y},\tau_3,\mathbf{x},2\tau_4,\mathbf{x},\tau_3,\mathbf{y},\tau_3)P(\tau_3,\mathbf{y},\tau_3,\mathbf{x},2\tau_4,\mathbf{x},\tau_3,\mathbf{y},\tau_3)P(\tau_3,\overline{\mathbf{y}},\tau_3,\overline{\mathbf{x}},2\tau_4,\overline{\mathbf{x}},\tau_3,\overline{\mathbf{y}},\tau_3)P(\tau_3,\overline{\mathbf{y}},\tau_3,\overline{\mathbf{x}},2\tau_4,\overline{\mathbf{x}},\tau_3,\overline{\mathbf{y}},\tau_3)$$

where $\{\overline{\mathbf{x}},\overline{\mathbf{y}}\} \equiv \{-\mathbf{x},-\mathbf{y}\}$. The delays are given by

$$\tau_1 = \tau_0(1-u), \quad \tau_2 = \tau_0(1+2u),$$
$$\tau_3 = \tau_0(1+u), \quad \tau_4 = \tau_0(1-2u),$$

where τ_0 is 5 μs in this paper. The cycle time t_c, defined as the total time of the sequence, is given by $\tau = 24\tau_0$. u is a dimensionless adjustable parameter, and is restricted such that none of the inter-pulse spacings becomes negative. To the zeroth order Magnus expansion, the above sequence realizes Hamiltonian uJ_0D_y and $uJ_0 = J$.

[S1] See supplementary online material.

[S2] P. Cappellaro, C. Ramanathan, and D. G. Cory, "Simulations of information transport in spin chains," Phys. Rev. Lett. **99**, 250506 (2007).

[S3] Paola Cappellaro, Lorenza Viola, and Chandrasekhar Ramanathan, "Coherent-state transfer via highly mixed quantum spin chains," Phys. Rev. A **83**, 032304 (2011).

[S4] Chandrasekhar Ramanathan, Paola Cappellaro, Lorenza Viola, and David G Cory, "Experimental characterization of coherent magnetization transport in a one-dimensional spin system," New J. Phys. **13**, 103015 (2011).

[S5] E. Rufeil-Fiori, C. M. Sánchez, F. Y. Oliva, H. M. Pastawski, and P. R. Levstein, "Effective one-body dynamics in multiple-quantum nmr experiments," Phys. Rev. A **79**, 032324 (2009).

[S6] Wenxian Zhang, Paola Cappellaro, Natania Antler, Brian Pepper, David G. Cory, Viatcheslav V. Dobrovitski, Chandrasekhar Ramanathan, and Lorenza Viola, "Nmr multiple quantum coherences in quasi-one-dimensional spin systems: Comparison with ideal spin-chain dynamics," Phys. Rev. A **80**, 052323 (2009).

[S7] U. Haeberlen and J.S. Waugh, "Coherent averaging effects in magnetic resonance," Phys. Rev. **175**, 453–467 (1968).

[S8] Ken Xuan Wei, Chandrasekhar Ramanathan, and Paola Cappellaro, "Exploring localization in nuclear spin chains," Phys. Rev. Lett. **120**, 070501 (2018).

[S9] Ken Xuan Wei, Pai Peng, Oles Shtanko, Iman Marvian, Seth Lloyd, Chandrasekhar Ramanathan, and Paola Cappellaro, "Emergent prethermalization signatures in out-of-time ordered correlations," Phys. Rev. Lett. **123**, 090605 (2019).

[S10] Gurneet Kaur and Paola Cappellaro, "Initialization and readout of spin chains for quantum information transport," New J. Phys. **14**, 083005 (2012).

[S11] Yu-Sze Yen and A. Pines, "Multiple-quantum nmr in solids," J. Chem. Phys. **78**, 3579–3582 (1983).